Appl. Phys. B 67, 351–356 (1998)

Applied Physics B
Lasers
and Optics

Broadly tunable difference-frequency spectrometer for trace gas detection with noncollinear critical phase-matching in $LiNbO_3$

M. Seiter, D. Keller, M.W. Sigrist

Swiss Federal Institute of Technology (ETH), Institute of Quantum Electronics, CH-8093 Zürich, Switzerland
(Fax: +41-1/633-1077, E-mail: seiter@iqe.phys.ethz.ch, sigrist@iqe.phys.ethz.ch)

Received: 16 March 1998/Revised version: 1 July 1998

Abstract. A broadly, continuously and rapidly tunable cw laser spectrometer based on difference-frequency generation in bulk $LiNbO_3$ is reported. Using an external cavity diode laser, tunable from 795 to 825 nm, and a cw diode-pumped Nd:YAG ring laser at 1064 nm, we produced narrowband mid-ir laser light between 3.16 and 3.67 μm. This broad tuning range of 440 cm^{-1} can be critically phase-matched by changing the external crystal angle within a range of only 0.4°. Even for a fixed crystal angle broadband phase-matching over 230 cm^{-1} was achieved. No realignment was required when tuning the laser over the whole wavelength range, which enabled the use of a compact 36-m multipass cell as gas chamber. The conversion efficiency could be improved by almost a factor of 3 by applying noncollinear instead of collinear phase-matching, resulting in 30 nW of idler power with good beam quality. Spectra of methane were recorded in laboratory air, which demonstrate the rapid and continuous broad tunability at high sensitivity, enabling sub-ppm detection. Finally, wavelength modulation spectroscopy at high resolution was applied as a promising tool for further inproving the performance of this laser spectrometer.

PACS: 42.65.Ky; 42.62.Fi

The atmospheric windows from 3 to 5 μm and 8 to 14 μm are the preferred spectral regions for trace gas detection within the mid-infrared wavelength range between 2 and 20 μm, where many molecules of interest show strong fundamental rovibrational absorptions. Difference-frequency generation (DFG) in nonlinear crystals, pumped by commercial single-frequency diode lasers and/or diode-pumped solid-state lasers in the visible or near infrared, has proven to be a useful technique for high-resolution infrared spectroscopy [1–7]. These DFG sources offer the benefits of reliability, compactness, no need of cryogenic cooling, low cost and low power consumption in combination with good amplitude and frequency stability. In these respects, they are superior to other tunable mid-ir laser sources, such as color-center lasers, lead-salt diode lasers [8] or sources based on sideband generation by CO and CO_2 lasers [9], which all suffer from their own specific practical drawbacks. Current developments on distributed feedback quantum cascade lasers [10] or solid-state lasers like Dy:$BaYb_2F_8$ [11] are promising, but still do not meet all of the above-mentioned requirements and are not yet commercially available.

For real-time, true multi-component capability of a DFG laser-based gas sensor a substantial continuous DFG laser tuning range is required with rapid scan and control possibility. Pine [12], who first reported on DFG for high-resolution spectroscopy, achieved a broad tuning range from 2.2 to 4.2 μm by temperature tuning of a $LiNbO_3$ crystal. However, this is a rather slow tuning scheme. Simon et al. [2] applied critical phase-matching in $AgGaS_2$, cut for 90° type-I phase-matching, using an external cavity diode laser (ECDL) near 795 nm and a diode-pumped Nd:YAG laser (frequency fixed at 1064 nm). To cover a wavelength range from 3.155 to 3.423 μm the internal phase-matching angle was varied between 90° and 75°, which yielded an external angle range of 38°. Recently, quasi-phase-matched DFG laser spectrometers have been developed that use periodically poled lithium niobate (PPLN) [3, 4]. Thus the largest nonlinear coefficient d_{33} in $LiNbO_3$ can be used. Goldberg et al. [13] achieved a continuous wavelength tuning range between 3.0 and 4.1 μm for a fixed grating period in PPLN. However, this arrangement requires a large angle range of 55° for grating rotation, which makes fast and accurate tuning across a broad wavelength range rather difficult. Furthermore, compensation for maintaining the beam direction would be necessary. In the range of 4.3–4.6 μm, Goldberg et al. [14] performed wideband phase-matching for a fixed phase-matching angle, which permits fast and stable wavelength tuning within this range. Töpfer et al. [5] used a multigrating chip of PPLN with eight stripes of different domain grating periods resulting in ideal phase-matching for eight narrow wavelength regions. Recently, developments have been reported on single-frequency cw optical parametric oscillators using such a multigrating PPLN chip as a nonlinear optical crystal and a diode-pumped Nd:YAG ring laser as a pump source [15]. Up to 140 mW of idler power in the mid-ir range were reported with a frequency stability of less than 10 MHz/min, making this laser source interesting for spectroscopic applications. However,

broad tuning had to be performed by changing the crystal periods and then adapting the temperature of the crystal between 110 and 150 °C. A small, mode-hop-free continuous tuning range of 2 GHz was achieved by varying the pump frequency through temperature control of the laser crystal.

The purpose of this work was to develop a compact, rapidly tunable DFG laser spectrometer by employing a cw diode-pumped Nd:YAG laser at 1064 nm and an external cavity diode laser (ECDL, tunable from 795 to 825 nm) as pump sources as well as a multipass cell as a gas chamber. The mid-ir radiation is continuously tunable in the range from 3.16 to 3.67 μm, where at least 60 of the 189 "hazardous air pollutants" (HAPs), which have been defined in the US Clean Air Act Amendments of 1990 [16], exhibit absorptions. At atmospheric pressure, many of these compounds (methanol, ethanol, benzene, toluene, etc.) show similar quasi-continuous absorption spectra. To analyze multicomponent mixtures of such molecules, a broad continuous tuning range must be available [17]. We apply critical phase-matching in bulk $LiNbO_3$ with the advantage of an ultranarrow range of the external angle, sufficient for achieving phase-matching over the whole tuning range. This results in a very stable beam direction of the generated idler wave, a crucial feature when a compact multipass cell is employed. A main drawback of critical phase-matching, however, is the walk-off between the pump and signal beams in the birefringent crystal, resulting in an order-of-magnitude lower conversion efficiency than for noncritical phase-matching [18]. Therefore, we investigated noncollinear phase-matching for walk-off compensation in view of power boosting by simultaneously maintaining beam quality. We report on the design and performance of this compact gas sensor with regard to gas analysis over broad spectral regions by monitoring samples of methane and natural laboratory air. Furthermore, we present spectra of methane with high resolution by applying direct absorption as well as wavelength modulation spectroscopy.

1 Diode-pumped, continuously tunable DFG source

Our experimental setup is illustrated by the schematic diagram in Fig. 1. Two compact lasers are used as pump and signal sources for the mixing process: an external cavity diode laser (ECDL) with an output power between 25 and 30 mW at wavelengths tunable from 795 nm to 825 nm (EOSI, Model 2010), and a cw diode-pumped monolithic Nd:YAG laser emitting up to 1 W in a single longitudinal mode at 1064 nm (Laserzentrum Hannover e.V., InnoLight GmbH). These lasers have linewidths of a few MHz (ECDL) and ∼ 1 kHz (Nd:YAG) resulting in a narrowband mid-ir laser source. The polarization of the Nd:YAG laser beam is changed from elliptical to linear by inserting a quarter-wave plate. A vertically polarized beam is then obtained by a half-wave plate, allowing type-I phase-matching in $LiNbO_3$ in combination with the horizontally polarized ECDL. The pump and the signal beam are overlapped by a polarizing beamsplitter after spatial mode-matching (lenses L_1, L_3 and L_4) and focused by the lenses L_2 ($f = 200$ mm) and L_5 ($f = 150$ mm), respectively. In an antireflection-coated (AR-coated) 7 mm × 7 mm × 25 mm $LiNbO_3$ crystal (Fujian Casix Laser, Inc.), cut at 46.5°, critical phase-matching is applied by rotating the crystal in the horizontal plane. The radiation of the pump and signal waves is removed by an AR-coated Germanium filter and the generated idler beam is collimated by the lens L_6 ($f = 200$ mm). After deflection by the mirrors M_1 and M_2 the idler beam is slightly focused by the lens L_7 ($f = 380$ mm) into the center of the multipass cell (type Heriott). The transmitted radiation is detected by a liquid-nitrogen-cooled InSb detector.

The phase-matching curve in $LiNbO_3$ for the employed pump and signal lasers is depicted in Fig. 2. The measured external crystal angle was recorded relative to phase-matching at a pump wavelength of 810 nm by counting the steps of the computer-controlled, motorized rotation stage (Owis, DMT40). A comparison with calculated data taken from well-known Sellmeier equations [19] is also shown. When the ECDL was tuned from 795 to 825 nm, the wavelength region between 3.16 and 3.67 μm was covered by varying the external angle within a range of only 0.4°. A characteristic feature and main advantage of critically phase-matched DFG in $LiNbO_3$ is the broad minimum around a pump wavelength of 815 nm. This fact allows wideband phase-matching of several hundred wavenumbers, since an angular acceptance bandwidth (FWHM) of greater than 0.06° was measured. Figure 3

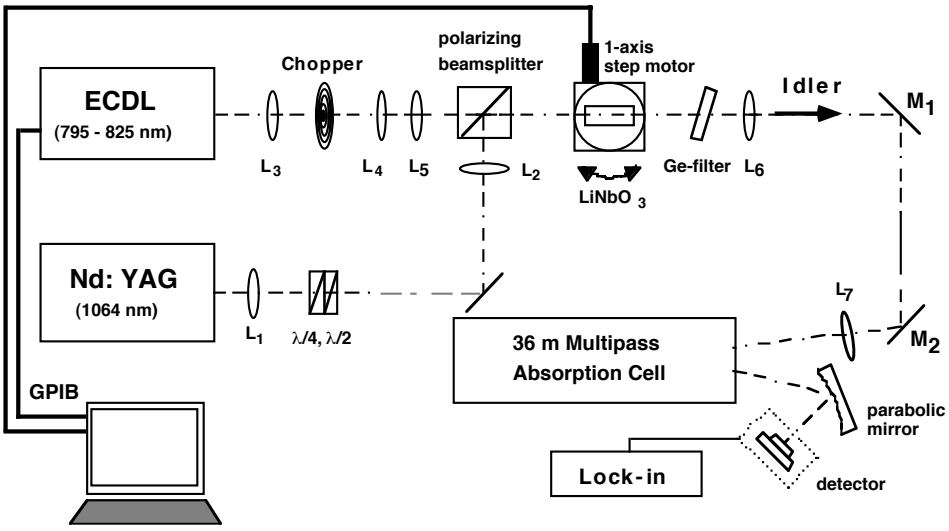

Fig. 1. Schematic diagram of compact DFG laser spectrometer pumped by a cw diode-pumped Nd:YAG laser at 1064 nm and a tunable external cavity diode laser (795–825 nm). The generated mid-ir radiation, tunable between 3.16 and 3.67 μm, is coupled through a 36-m multipass cell via the mirrors M_1 and M_2. L_1 to L_7, lenses; λ/2, half-wave plate; λ/4, quarter-wave plate. Spectra are recorded by a liquid-nitrogen-cooled InSb detector. Both the ECDL and the rotation stage for the $LiNbO_3$ crystal are controlled by a computer via GPIB

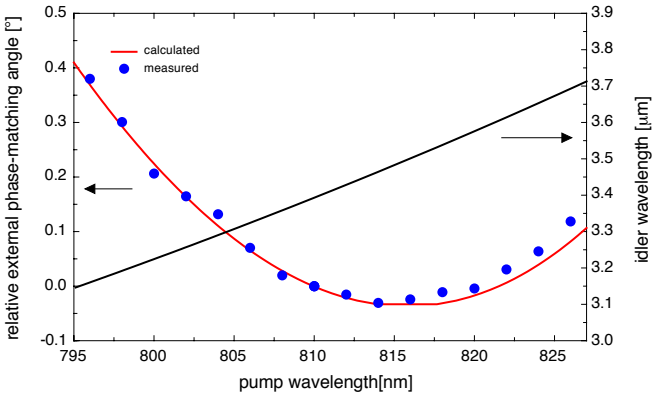

Fig. 2. Type-I phase-matching curve (*left ordinate*) for bulk $LiNbO_3$, cut at an angle of 46.5° with respect to the optic axis. The broad minimum in this curve results in an ultranarrow angular range of only 0.4°, which is sufficient for achieving phase-matching over the whole idler tuning range between 3.15 and 3.7 μm (*right ordinate*). The measured data points agree well with the calculated *solid line* based on Sellmeier equations

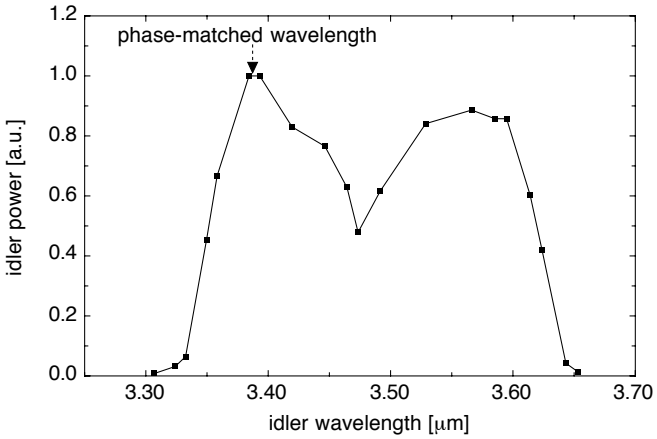

Fig. 3. Tuning curve demonstrating wideband phase-matching over nearly 300 nm in the mid-ir without any crystal rotation. This *curve* was recorded at a fixed phase-matching angle optimized for a pump wavelength of 810 nm as indicated

shows a tuning curve for a fixed phase-matched wavelength covering an idler range from 3.35 to 3.63 μm without any crystal rotation. The minimum in the center of this curve at 3.48 μm corresponds to the minimum in the phase-matching curve of Fig. 2 at a pump wavelength near 815 nm. A very interesting, broad spectral range for trace gas analyses can thus be accessed, and fast scans can be performed at a stable direction of the generated mid-ir beam. By adapting the phase-matched wavelength, the tuning curve of Fig. 3 can be shifted towards shorter or longer wavelengths, which changes the shape and hence the width of the curve.

These advantages of critical phase-matching in $LiNbO_3$ are achieved at the expense of a poor conversion efficiency caused by Poynting vector walk-off ($\varrho = 2.2°$) between the extraordinary pump and the ordinary signal waves inside the crystal. In order to compensate for this walk-off, we investigated noncollinear phase-matched DFG in view of a mid-ir laser source useable for spectroscopy. Figure 4 shows the wave vectors and Poynting vectors of the three interacting waves in the crystal. When the wave vectors of the pump and signal waves propagate at an angle (ϱ) of 2.2° with respect to

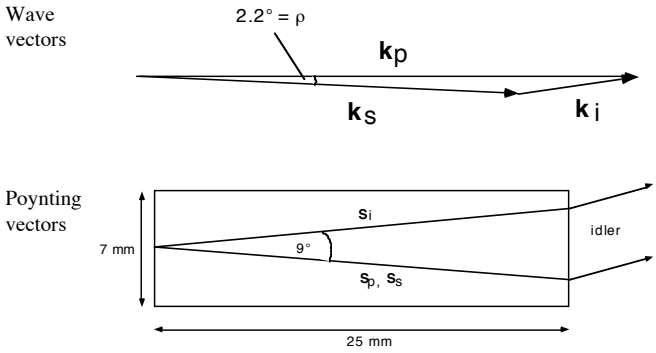

Fig. 4. Noncollinear phase-matching in $LiNbO_3$ for full compensation of the pump walk-off. The wave vectors of the pump and signal beams propagate at 2.2° (walk-off angle) with respect to each other inside the crystal (*upper diagram*). As a result, the Poynting vectors S_p of the pump and S_s of the signal beams coincide within the crystal, whereas the Poynting vector S_i of the generated idler beam walks off at an angle of 9° (*lower diagram*). The crystal used had a length of 25 mm and a width of 7 mm

each other, walk-off is fully compensated, which is deduced from the fact that the signal and pump beams enter and leave the crystal at the same spots on the front and back facet of the crystal. To realize this "strong" noncollinear phase-matching, the polarizing beamsplitter (Fig. 1) was replaced by a mirror deflecting the signal beam so much that it entered the crystal at an angle of $\alpha = 5°$ with respect to the pump beam, which itself was not affected by the mirror. In this configuration the phase-matching angles in $LiNbO_3$ were shifted towards higher values around 50° to the optic axis. A four-times-higher conversion efficiency was achieved for this fully walk-off compensated, noncollinearly phase-matched DFG compared with collinear phase-matching. The generated idler beam propagated, however, at an angle of $\Phi = 9°$ with respect to the overlapping pump and signal waves inside the crystal. This resulted in a larger diameter of the idler beam (Fig. 4) and a still lower conversion efficiency than would be obtained for noncritical (90°) phase-matching. In order to calculate the conversion efficiency for noncollinearly phase-matched DFG, the physical crystal length L has to be substituted by an effective length L_{eff} [20]:

$$L_{\text{eff}} \propto \left(\frac{L w}{\sin \Phi}\right)^{\frac{1}{2}} , \qquad (1)$$

where w represents the diameter of the pump and signal beam and Φ the walk-off angle of the idler beam. We have employed an uncoated 50-mm-long $LiNbO_3$ crystal and obtained a 1.4-times-higher conversion efficiency than for the 25-mm-long crystal as predicted by (1). The dependence of L_{eff} on w and Φ illustrates that the introduced decreasing overlap between the idler and pump waves (idler walk-off) limits the possible gain in the generated output power. When the pump and signal beams were focused to a spot radius of approximately 100 μm into the middle of the crystal, the maximum idler power was obtained at an angle $\alpha \approx 4.1°$ as a trade-off between idler walk-off and pump walk-off. We investigated the influence of these two effects by further decreasing the angle α between the incident pump and signal beam. Figure 5 shows the dependence of the obtained conversion efficiency on α. The measured points for $\alpha > 1°$ (strong noncollinear regime) have been recorded in the configuration using the

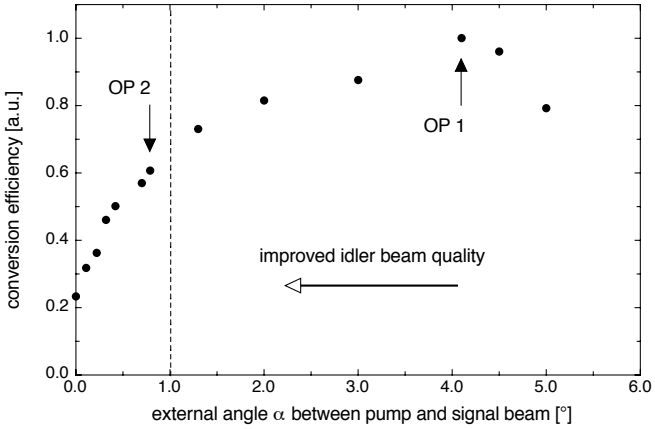

Fig. 5. Conversion efficiency by noncollinear phase-matching in $LiNbO_3$ (normalized to 1.0 at operation point OP 1). An angle of $\alpha = 5°$ between pump and signal beams outside the crystal fully compensates pump walk-off. Maximum conversion efficiency is achieved at $\alpha = 4.1°$ (OP 1). For $\alpha = 0.8°$ (OP 2) an almost three times higher conversion efficiency is obtained compared with collinear phase-matching ($\alpha = 0°$) at still good beam quality. The configuration at OP 2 was used for sensitive absorption spectroscopy in combination with the 36-m multipass cell

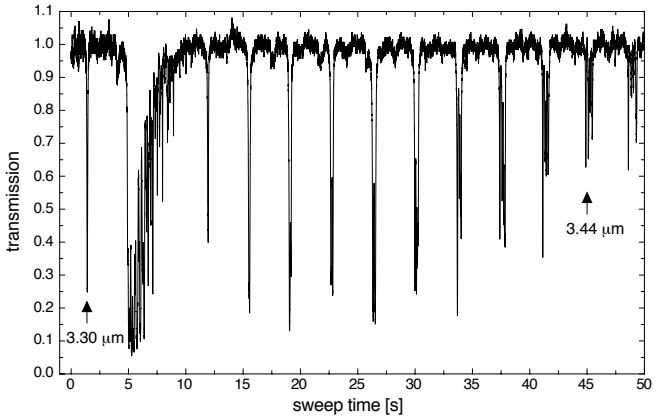

Fig. 6. Transmission spectrum of 500 ppm methane buffered in air at atmospheric pressure in a 1-m two-pass absorption cell. The single scan demonstrates the broad and rapid continuous tunability of our DFG laser source. Data were recorded by an InSb detector located after the absorption cell and read out via a lock-in amplifier (bandwidth 30 Hz). A scan rate of 0.2 nm/s was applied to the ECDL

mirror instead of the beamsplitter (Fig. 1). Angles $\alpha < 1°$ (weak noncollinear regime) were achieved by slightly rotating the beamsplitter in the initial setup according to Fig. 1. Since the pump walk-off played a more important role in the weak regime than in the strong noncollinear regime, the beams were focused to a larger spot size of approximately 300 μm for $\alpha < 1°$, compared with 100 μm for $\alpha > 1°$. We have selected two operating points, denoted as OP 1 and OP 2 in Fig. 5, at which to perform spectroscopic studies. On the one hand, we have used the maximum output power at $\alpha = 4.1°$ (OP 1). With ideally coated optics, an estimated power of 150 nW could be achieved if 900 mW of signal and 27 mW of pump power were incident on a 50-mm-long AR-coated crystal. In practice, only approximately 45 nW were obtained due to nonideally coated optics and the use of an uncoated crystal. It should be noted, however, that the idler beam quality at OP 1 is rather poor and was thus only used in combination with a 1-m two-pass absorption cell. On the other hand, we have chosen an angle α just below 1° (OP 2) as a trade-off between idler power and beam quality. Although the conversion efficiency, and thus the idler power, at OP 2 is lower than at OP 1, it is still three times higher than the collinear phase-matched DFG (see Fig. 5). With 750 mW of signal and 22 mW of pump power incident on a 25-mm-long AR-coated crystal, more than 30 nW of idler power could be generated. In contrast to the situation at OP 1, a good beam quality is now obtained, comparable to that of collinear phase-matched DFG. Hence, our 36-m multipass cell could be employed to record absorption spectra with high sensitivity.

2 Spectroscopic studies

A 50-cm-long gas cell (2 passes) was filled with ∼ 500 ppm methane buffered in natural air of atmospheric pressure to perform spectroscopic measurements using the walk-off compensated noncollinearly phase-matched DFG source (OP 1 in Fig. 5). Figure 6 shows the spectrum of the Q and P branches (rovibrational transitions) of the asymmetric stretch mode ν_3 recorded by a liquid-nitrogen-cooled InSb detector in combination with a lock-in amplifier at a chopper frequency of 1.3 kHz (see Fig. 1). A single sweep was performed by applying a scan rate of 0.2 nm/s to the ECDL at start and stop wavelengths of 804 and 814 nm, respectively. A spectral range from 3.30 to 3.45 μm in the mid-ir was covered by a single scan in 45 s at a fixed crystal angle, demonstrating the broad continuous tunability. The single lines within the Q and P branches are clearly resolved.

In order to increase the sensitivity of our laser spectrometer, we substituted the 1-m absorption cell by a compact multipass cell (New Focus, Model 5611). The two astigmatic mirrors of this cell are separated by 20 cm in a cell volume of 300 cm^3. After 182 passes, the incident beam leaves the cell through the same hole (of 2.5 mm diameter, yielding a 36-m optical path length). Therefore, ir radiation of good beam quality and stable beam direction is crucial. For this reason, we operated our DFG laser source in the weak noncollinear regime at OP 2 (Fig. 5) with a power of ∼ 30 nW. After collimation of the idler beam (lens L_6 with $f = 200$ mm, Fig. 1) an almost circular beam shape was obtained with a diameter of approximately 3 mm, which could easily be focused into the center of the multipass cell by L_7 ($f = 380$ mm, Fig. 1). The measured throughput of the cell over 3–4 μm was approximately 14% after 181 reflections by the cell mirrors. Thus, several nanowatts were still available for recording the absorption spectra with the InSb detector with a noise equivalent power of several 10 $pW/Hz^{1/2}$, supplying sufficient signal-to-noise ratio.

Figure 7 shows a measured spectrum of natural laboratory air at atmospheric pressure between 3011 and 3024 cm^{-1}. A scan rate of 0.1 nm/s was applied to the ECDL, yielding 10 s for a single sweep. With a bandwidth of 10 Hz, set at the lock-in amplifier, the spectrum was obtained by averaging 20 sweeps. To normalize the spectrum near 3020 cm^{-1}, where no absorptions occurred, the baseline was recorded by reflecting the mid-ir radiation onto the same detector via a flipper mirror, which was located just in front of the multipass cell.

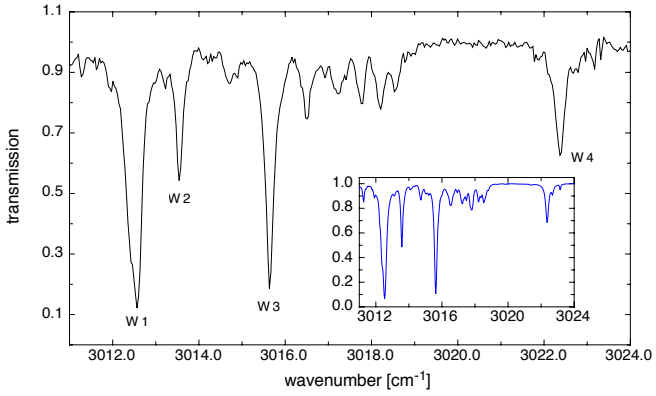

Fig. 7. A 20-sweep average over the spectrum of natural laboratory air at atmospheric pressure. Lock-in bandwidth was 10 Hz. A single sweep was recorded in 10 s. The *water lines*, W 1–W 4, were used for wavenumber calibration. The other absorption lines belong to the Q branch of the ν_3 asymmetric stretch vibration of methane. The measured spectrum agrees well with a computed spectrum (Hitran database [21]) of 1.7 ppm methane and 0.775% water vapor in air, as illustrated by the *inset*

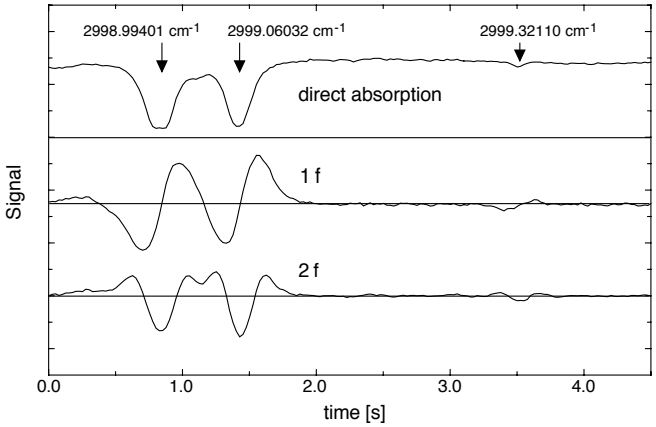

Fig. 8. Comparison of direct absorption (*upper trace*), $1f$- (*center*) and $2f$-signal (*bottom trace*) of 100 ppm methane buffered in 60 mbar air. The three signals are offset vertically for clarity including the *zero lines* of each trace. The spectra were recorded as an average of 20 sweeps over approximately 16 GHz by applying a triangle voltage to the PZT. Lock-in bandwidth was 10 Hz. Modulation frequency f and amplitude for wavelength modulation ($1f$, $2f$) were 1.2 kHz and 0.75 GHz, respectively

The wavenumber axis was calibrated by using the strong water absorptions (W 1–W 4 in Fig. 7) as references. Apart from these water lines, many methane absorptions, which belong to the Q branch of the ν_3 asymmetric stretch vibration, could be detected. The inset in Fig. 7 shows the computed spectrum for concentrations of 1.7 ppm methane (corresponding to the natural abundance in air) and 0.775% of water vapor at atmospheric pressure. This computation is based on Hitran data [21] and was performed for an optical path length of 36 m. It illustrates the good agreement with the measured spectrum. According to the observed signal-to-noise ratio (Fig. 7) of greater than 8, we are currently able to detect concentrations of methane in natural air down to the sub-ppm range (< 200 ppb).

In addition to these spectral studies over broad continuous wavelengths ranges, spectral measurements were performed at higher resolution by applying the fine-tuning mode of our ECDL. A continuous tuning range of up to 70 GHz can be covered by changing the voltage to the piezo transducer (PZT). Modulation frequencies up to several kHz can be applied to the PZT. Wavelength modulation spectroscopy (WMS) can thus be performed, which is often advantageous. Figure 8 shows a 20-sweep average over a spectral range containing three absorption lines of 100 ppm methane buffered in 60 mbar of synthetic air near 2999 cm^{-1}. The sweep rate was approximately 3.6 GHz/s. In order to perform wavelength modulation spectroscopy (middle and bottom traces of Fig. 8) a sine voltage with a frequency of $f = 1.2$ kHz was applied to the PZT in addition to the triangle voltage responsible for the wavelength scan. The first and second derivatives of the absorption profiles were then recorded via a lock-in technique by detecting the first and second harmonics, respectively. No chopper was needed in this case. In order to compare these three signals (direct absorption, $1f$, $2f$) the traces have been offset vertically for clarity, including the zero lines for each trace. The three signals were all recorded with the same sensitivity of the lock-in amplifier. The slow baseline slope, which can represent a problem in the direct absorption signal, is completely eliminated in the $2f$-signal. Consequently, the weak transition (01100112 – 00000000) at 2999.32110 cm^{-1} with a line intensity of $S = 6.41 \times 10^{-22}$ $\mathrm{cm}^{-1}/(\mathrm{molecule\ cm}^{-2})$, approximately 50 times weaker than the one at 2999.06032 cm^{-1}, can be clearly distinguished from noise due to the characteristic shape of an absorption line in the $2f$ mode.

3 Conclusions

We have developed a broadly tunable mid-ir laser source that is well suited for spectroscopic applications and uses a compact multipass cell. By using a tunable external cavity diode laser near 810 nm and a cw diode-pumped Nd:YAG ring laser at 1064 nm, mid-ir radiation, continuously tunable between 3.16 and 3.67 μm, with an output power of ~ 30 nW is produced by difference-frequency generation. The direction of the generated idler beam is kept very stable over the whole tuning range by applying critical phase-matching in $LiNbO_3$. Since no crystal rotation at all is required over a broad range of almost 300 nm in the mid-ir, fast and excessive wavelengths scans can be easily performed. Thus, this laser source should be a promising tool for analyses of multicomponent mixtures of gases, which often exhibit overlapping absorption spectra at atmospheric pressure.

The issue of collinear and noncollinear phase-matching was studied in detail with respect to walk-off effects in the birefringent $LiNbO_3$ crystal. As a trade-off between power and beam quality of the generated idler wave we have chosen a weak degree of noncollinearity, resulting, nevertheless, in an idler power almost three times higher than that obtained with exact collinear phase-matching, at still good beam quality.

Furthermore we have proven that our compact laser spectrometer is capable of recording spectra with high resolution by applying various detection modes, namely direct absorption, $1f$- and $2f$- spectroscopy. The narrow linewidth combined with the broad tuning range can be exploited for high selectivity between different gases in multicomponent mixtures. From the extracted signal-to-noise ratio of absorption spectra of natural air we deduced a detection limit for me-

thane in air in the sub-ppm range, well below its natural abundance.

Nevertheless, the enhancement of the still rather low signal-to-noise ratio is one of the key issues for further improving the detection limit and accuracy of our spectrometer. Several measures will be taken to achieve this goal. First, a thermoelectrically cooled detector with even lower noise equivalent power of some $pW/Hz^{1/2}$ will be employed. Furthermore, the output power of the mid-ir laser source can be boosted by implementing a build-up cavity around the $LiNbO_3$ crystal, which is resonant for the signal wave. Here, again advantage can be taken of the ultranarrow angle range of 0.4° for phase-matching. This makes any realignment of cavity mirrors or compensation of beam direction unnecessary while tuning the laser.

Acknowledgements. This work was supported by the priority program "OPTIQUE II" of the board of the Swiss Federal Institutes of Technology. The collaboration with ECO PHYSICS (Switzerland) and Laserzentrum Hannover e.V./InnoLight GmbH (Germany) is acknowledged.

References

1. U. Simon, Z. Benko, M.W. Sigrist, R.F. Curl, F.K. Tittel: Appl. Opt. **32**, 6650 (1993)
2. U. Simon, S. Waltman, I. Loa, F.K. Tittel, L. Hollberg: J. Opt. Soc. Am. B **12**, 323 (1995)
3. K.P. Petrov, L. Goldberg, W.K. Burns, R.F. Curl, F.K. Tittel: Opt. Lett. **21**, 86 (1996)
4. K.P. Petrov, S. Waltman, E.J. Dlugokencky, M. Arbore, M.M. Fejer, F.K. Tittel, L.W. Hollberg: Appl. Phys. B **64**, 567 (1997)
5. Th. Töpfer, K.P. Petrov, Y. Mine, D. Jundt, R.F. Curl, F.K. Tittel: Appl. Opt. **36**, 8042 (1997)
6. W. Schade, T. Blanke, U. Willer, C. Rempel: Appl. Phys. B **63**, 99 (1996)
7. B. Sumpf, T. Kelz, M. Nägele, H.-D. Kronfeldt: Appl. Phys. B **64**, 521 (1997)
8. M.W. Sigrist (Ed.): *Air Monitoring by Spectroscopic Techniques*, Chemical Analysis, Vol. 127, Chap. 5 (Wiley, New York 1994)
9. S.C. Hsu, R.H. Schwendeman, G. Magerl: IEEE J. Quantum Electron. **QE-24**, 2294 (1988)
10. J. Faist, C. Gmachl, F. Capasso, C. Sirtori, D.L. Sivco, J.N. Baillargeon, A.Y. Cho: Appl. Phys. Lett. **70**, 2670 (1997)
11. N. Djeu, V.E. Hartwell, A.A. Kaminskii, A.V. Butashin: Opt. Lett. **22**, 997 (1997)
12. A.S. Pine: J. Opt. Soc. Am. **64**, 1683 (1974)
13. L. Goldberg, W.K. Burns, R.W. McElhanon: Opt. Lett. **20**, 1280 (1995)
14. L. Goldberg, W.K. Burns, R.W. McElhanon: Appl. Phys. Lett. **67**, 2910 (1995)
15. K. Schneider, P. Kramper, S. Schiller, J. Mlynek: Opt. Lett. **22**, 1293 (1997)
16. T.J. Kelly, R. Mukund, Ch.W. Spicer, A.J. Pollack: Environ. Sci. Technol. **28**, 378 (1994)
17. A. Bohren, M.W. Sigrist: Infrared Phys. Technol. **38**, 423 (1997)
18. Y.-R. Shen (Ed.): *Nonlinear Infrared Generation* (Springer, Berlin, Heidelberg 1977)
19. G.J. Edwards, M. Lawrence: Opt. Quantum Electron. **16**, 373 (1984)
20. B. Lax, R.L. Aggarwal, G. Favrot: Appl. Phys. Lett. **23**, 679 (1973)
21. L.S. Rothman, R.R. Gamache, R.H. Tipping, C.P. Rinsland, M.A.H. Smith, D. Chris Benner, V. Malathy Devi, J.-M. Flaud, C. Camy-Peyret, A. Perrin, A. Goldman, S.T. Massie, L.R. Brown, R.A. Toth: J. Quant. Spectrosc. Radiat. Transfer **48**, 469 (1992)